12-15-2007

Magneto-Optical Study of Cobalt Ferrite Nanoparticles

Byron L. Scott
University of New Orleans

Magneto-Optical Study of Cobalt Ferrite Nanoparticles

A Thesis

Submitted to the Graduate Faculty of the
University of New Orleans
in partial fulfillment of the
requirements for the degree of

Master of Science
in
Applied Physics

by

Byron L. Scott

B. S., University of New Orleans, 2003

December 2007

ACKNOWLEDGMENTS

I would like to give my sincerest thanks to Dr. Kevin Stokes, who been at my side through much more than the scope of this thesis. From rebuilding a chemistry lab on the second floor to rebuilding my life at least twice, Dr. Stokes somehow allowed me pursue my goal as a scientist as it would not have been possible for me to accomplish this with any other advisor. I extend my gratitude to the entire faculty at the Advanced Materials Research Institute, including Dr. Leonard Spinu, Dr. Weilie Zhou, and Cosmin Radu for allowing us access to their equipment. Thanks to Sandra Merz for everything.

TABLE OF CONTENTS

LIST OF FIGURES

ABSTRACT

A magneto-optical study of $Co_xFe_{1-x}Fe_2O_4$ nanoparticles is presented, with cobalt molar ratio $0 \leq x \leq 1$. The ferrite nanoparticles were produced using a generic wet-chemical synthesis procedure. Stoichiometric amounts of Fe^{2+}, Fe^{3+} and Co^{2+} salts are dissolved in a non-aqueous polar medium (diethylene glycol). A coprecipitation reaction with sodium hydroxide produces ferrite nanoparticles with average diameter of 6 nm. The nanoparticles can be stabilized by tetramethyl ammonium hydroxide in water, or, alternatively, the nanoparticles can be treated with a hydrophobic capping ligand with a carboxylic acid or amine head group and suspended in a non-polar organic solvent. As a complete structural analysis of this series of samples is quite difficult due to the similarities of the constituents, magneto-optical spectroscopy is performed to decode the structural orientations of each cation involved. Faraday rotation was measured on nanoparticle samples dried on an amorphous silica substrate from 400-1000 nm.

Chapter 1 - INTRODUCTION

1.1 Overview

Magneto-optical effects and the reasons they occur have been studied fairly vigorously for the last 160 years. The first magneto-optical phenomenon was discovered by Michael Faraday in 1845.[1] Faraday, drawing on some of his previous research with refractive indices and his interest concerning the interaction of electric and magnetic fields in matter, shined a beam of linearly polarized light on a prism of high refractive index under an applied electric field in hopes of observing some change in the medium or transmitted light. Faraday observed nothing and decided, with the aid of Lord Kelvin, to apply a magnetic field to the sample instead. The lines of magnetic force were parallel to the optic axis and perpendicular to the prism (polar configuration) and Faraday's hypothesis was confirmed as the plane of polarization of the beam of light was rotated by an angle, θ_F, upon transmission through the sample, no matter the direction of propagation of the incident beam. This discovery, now called the Faraday Effect, eventually led him to classify materials based on their magnetic properties (Sec 1.2). In 1875, eight years after Faraday's death, Scottish physicist John Kerr applied similar experimental parameters as Faraday except that for Kerr's experiment, the incident beam was reflected from the sample.[1] The reflected beam was rotated by twice the Faraday rotation angle, $2\theta_F$, and this phenomenon is called the Kerr effect (often, the Magneto-Optical Kerr Effect or MOKE). Similar rotations are also observed, though not as outstanding, when the magnetic force lines are perpendicular the optic axis and are referred to as the Cotton-Mouton effect for liquids and the Voigt effect for gaseous samples.[2]

This thesis deals with the magneto-optical Faraday effect in nanoparticles of a class of magnetic oxides, known as ferrites. In particular, the ferrites in this study are of the spinel group. A large number of metal oxides with the metal to oxygen ratio of 3:4 are known to crystallize in the spinel structure.[3] The general chemical formula of these materials is $M_xFe^{II}_{1-x}Fe^{III}_{2}O_4$ where M is a divalent cation, Fe^{II} indicates iron in its divalent state and Fe^{III} indicates iron is in its trivalent state. Specifically, we study the family of compounds with cobalt as the divalent cation M, with molar concentration of cobalt from x=0.0 to x=1.0.

Spinel ferrites are some of the most widely used materials in the world. The most famous of the ferrites, magnetite, is the strongest naturally occurring magnet and has been a topic of interest for hundreds of years. Magnetite, Fe_3O_4, was the first to find a commercial application as it was used as a lodestone by early navigators to locate magnetic north. Ferrites have numerous modern commercial applications including radio receiver antennae, ferrite-cored inductors, and magneto-optical recording materials.[2,4,5]

Cobalt ferrite ($CoFe_2O_4$) and magnetite (Fe_3O_4) are ferrimagnetic oxides with an inverse spinel structure. Although the properties of bulk ferrites have been studied extensively,[3] nanometer-scale ferrites display interesting magnetic and magneto-optical effects which have yet to be fully investigated. Among these are quantum confinement of itinerant electrons,[6] photomagnetic effects,[7] and near-field optical interactions.[8,9] Recently, cobalt ferrites have been studied for possible room temperature, spin-filter applications due to there high Curie temperature and good electrical insulation properties.[10,11] In addition, bulk ferrites have high cubic anisotropy and high coercivity which makes nanophase ferrites potentially useful for magnetic data storage applications. Flexible composites containing superparamagnetic nanoparticles may also find applications in magnetic shielding and flux concentrators. This

motivates us to develop a generic procedure capable of producing a full-range of ferrite samples with controllable magnetic moments and magneto-optical properties in the visible region.

As the focus of the work deals with Faraday rotation from a series of magnetic nanoparticles, some insight into the properties of magnetic materials will now be established. The remainder of this section will detail the classification of a particular group of magnetic oxides, known as ferrites and discuss the structural properties of one particular group of ferrites, the spinel group. Chapter 2 is a theoretical explanation of the causes of the Faraday Effect, including the induced circular birefringence of a given material and proposed electronic transitions initiated by the incident light. Details of both the chemical synthesis of these samples and the techniques applied in determining their properties is presented in Chapter 3. Chapter 4 displays the results from all experiments and analyses with subsequent discussion of all observations immediately following in Chapter 5. Chapter 6 conveys a conclusion from this research and presents some possible directions for further research.

Ferrites

1.2 Ferrimagnetism

Materials are often categorized by the nature of their magnetic properties. Among the different classes of magnetic materials are diamagnets, paramagnets, and magnetically ordered magnetic materials (or magnetic) with, as one would expect, a few subclasses. These three classes are distinguished by the degree and orientation of magnetic ordering in a particular material. When organizing into a crystal lattice, a given cation has some options regarding the placement of its

valence electrons. Electrons are first placed one by one in the ground state orbitals. A representative crystal field diagram for a d^3 cation in an octahedral crystal field is shown below

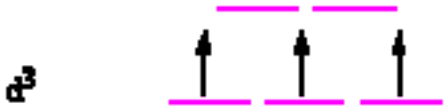

Figure 1.1 Crystal field diagram for a d^3 cation

After each of these ground state orbitals contains one electron, the placement of the fourth electron is determined by the amount of energy required to occupy the upper-level states, dq, vs. the amount of energy required to pair this electron with another in the ground state, E_p. The lower of these two values corresponds to the location of the next electron. If $dq \sim E_p$, this situation is referred to as a high-spin, low-spin crossover where the cation of interest changes its preferential orientation in the crystal lattice. As will be discussed presently, this orientation is paramount in establishing the magnetic and magnetic-optical properties of the sample. Magnetization is defined as the average magnetic moment per unit volume. In diamagnets, paramagnets and superparamagnets magnetization is essentially the response of the magnetic moments of atoms in a sample to an applied magnetic field. Magnetically ordered materials have spontaneous magnetization, but macroscopic samples tend to split into domains and the magnetization of the sample is due to domain processes such as magnetization rotations, nucleation and domain wall motion, A cooperative response indicates ferromagnetic or antiferromagnetic behavior where electrons in the sample are coupled by exchange interaction. This exchange coupling is a consequence of the atoms in the sample establishing the lowest energy equilibrium possible when forming a crystal lattice. In a ferromagnet, electrons are

largely unpaired and thus establish equilibrium by balancing their repulsive Coulomb interactions accordingly. For example, Fe^{3+} is an ideal ferromagnet where all *d*-orbitals are occupied by only one electron.

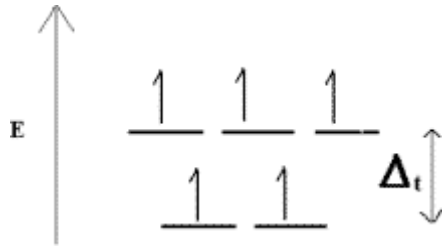

Fig. 1.2 CF Diagram for tetrahedral Fe^{3+}

Once the crystal lattice has been formed and all ions are satisfied, the lattice is now much more than just a collection of ions but, in fact, a series of unpaired electrons acting together to remain in their current situation with respect to their neighboring electrons. The results of this coupling are magnetic domains in the sample that respond cooperatively to an applied magnetic field. However, the magnetization of an entire domain does not cease to exist when the external field is removed. Rather, there exists an effective net magnetization as it takes a considerable amount of time and/or energy for the entire domain to return to its original state. This residual magnetization is characteristic of a true ferrite and is known as coercivity. Some elemental ferromagnets are shown in Fig. 1.3.

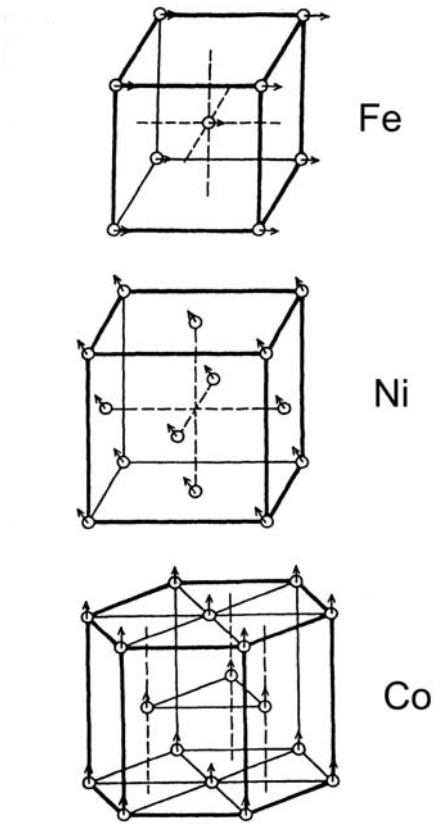

Figure 1. 3 Spin alignment in elemental ferromagnets.[4]

While this exchange coupling its quite strong, it may be destroyed with enough thermal excitation. When the temperature of the sample is raised enough so that all exchange coupling is insignificant, the Curie temperature, T_C, has been reached and the sample is no longer a ferromagnet but a paramagnet.

The view established previously holds for paramagnets as well. Paramagnets are often materials containing transition metals with some unpaired electrons. A paramagnetic crystal lattice may be described as crystal lattice with little to no exchange coupling and random distribution resulting in no significant magnetic ordering. Paramagnets do not display any residual magnetization and return to their origin almost immediately when the external field is removed but their overall

response is in the direction of the magnetic field. Superparamagnetism is a phenomenon displayed by materials that become paramagnetic at temperatures lower than T_C. Superparamagnetism is a condition that exists for ferromagnets with very small crystallite sizes. With the crystallites being extremely small, 0-20 nm, the range of the magnetic domains cannot exceed the size of the particles so the amount of electrons that can be coupled to each other is limited to only those in the crystallite. While the atoms in one particle may be coupled together, the particles are not coupled with each other and the thermal excitations can constantly randomize directions of the magnetizations of the particles. This behavior is undesirable for the magnetic data storage and is of great concern regarding the future of storage media as the magnetic bits of information approach tens of nanometers. A *superparamagnetic limit* exists where the particles on the disk must stay above this limit in order to preserve the ferromagnetic qualities of the material on the disk. Increased anisotropy and coercivity of magnetic materials is the way to push the superparamagnetic limit towards higher temperatures and secure information on magnetic discs. The converse of a paramagnet is a diamagnet where electrons in the sample are usually paired and the materials response is in opposition to the magnetic field. Diamagnets display no coercivity and thus, no exchange coupling. The behaviors of magnets, in general, may be further clarified by some inspection of equation 2.6.

While ferromagnets are the most widely known magnetics, there are other types of magnetically ordered materials, most notably those declared “antiferromagnets” by French physicist Louis Nèel in 1948. The mechanism for antiferromagnetism is very similar to that of ferromagnetism however the exchange interactions tend to align neighboring magnetic moments (spins) antiparallel. An antiferromagnet can be represented by two sublattices of magnetic moments with

magnetizations in opposite directions. In some antiferromagnets different magnetic atoms, M, or ions, M^{n+} located on different lattice sites, A and B.[12] These sites are collectively referred to as A and B sublattices. Although A and B may be any of several types of lattice sites, they are assumed here to be tetrahedral and octahedral sites in a close-packed structure. Where the ferromagnetic description involved nearly all electrons aligned the same, the antiferromagnet has the same type of magnetic ordering but is comprised of two components that oppose each other. All susceptible electrons on the A sublattice align parallel with each other while the same alignment occurs for all those on B sites resulting in a separate magnetic domain for each sublattice independently. However, the spins on tetrahedral sites are antiparallel to the spins on octahedral sites resulting in a net magnetization of zero if all susceptible electrons are equivalent.

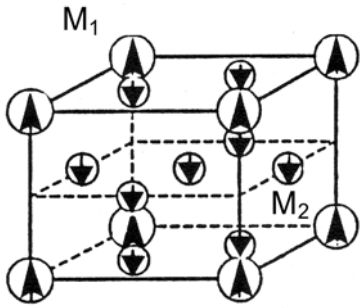

Figure 1.4 Atomic arrangement in a ferrimagnet. M_1 and M_2 atoms reside on different sublattices. If the spins from M_1 and M2 cancel exactly, then the materials is an "antiferromagnet."[12]

The validity of this mechanism is easily realized if one recalls some simple electron selection rules; namely, two electrons cannot coexist in the same orbital with the same spin state.[13] This results in the pairing of electrons with antiparallel spins in a given suborbital.[13] While the goal of this paper is not to prove these selection rules, this view serves as an adequate model for the alignment of antiparallel spins from different lattice sites. Although it may seem that all antiferromagnets exhibit zero net magnetization, a special case of this phenomenon is observed when different species occupy A and B. Antiferromagnets are also temperature dependent and

lose their magnetic ordering above a certain temperature to become paramagnetic. This temperature is referred to as the Neel temperature for antiferromagnets but differs only in name with the Curie temperature. With M_1 on A and M_2 on B, where M_1 and M_2 are just different types of atoms or cations, the susceptibilities of the sublattices are no longer equal, resulting in a nonzero net magnetization (see Fig. 1.4). This type of magnetic behavior, called "ferrimagnetism," has been labeled as such because it appears, almost exclusively, in a group of magnetic materials called "ferrites." If the two sublattices have different Curie temperatures the temperature dependence of magnetization is characterized by Neel and Curie temperatures which describe the transition from antiferromagnetic to ferromagnetic and form ferro- to paramagnetic state, respectively. Ferrites, an important group of magnetic materials, are applied throughout modern history to more problems than can be named here. While there are several types of ferrites, the focus here is on spinel ferrites where the general formula is MO: Fe_2O_3 and M is some divalent transition metal.

1.3 Spinel-Type Ferrites

All spinel ferrites consist of at least one type of divalent transition metal cation, M^{2+} and Fe^{3+} ions. Spinel refers to a special type of cubic close-packed (ccp) structure that all of these ferrites have in common where different cations are on different lattice sites. These different lattice sites are established by ccp layers of oxygen with M^{2+} and Fe^{3+} coordinated tetrahedrally or octahedrally to the surrounding oxygen layers. Tetrahedral coordination refers to a cation with four oxygen ions as nearest neighbors while a cation with octahedral coordination will be shared

among six. The coordination site is very important for our purposes due to differences in the electronic energy levels for a given atom on each lattice site (Sec. 2.3).

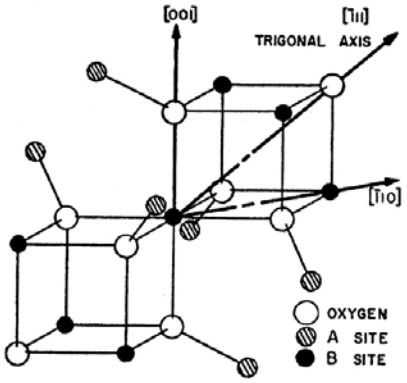

Figure 1.5 Spinel crystal structure. The occupation of the A and B sites by the M^{2+} and M^{3+} ions determine whether the structure is "normal" or "inverse" spinel.[14]

A material with the normal spinel structure has M^{2+} on tetrahedral sites and Fe^{3+} on octahedral sites, $(M^{2+})[Fe^{3+}]$, while the inverse spinel is considerably different in that M^{2+} has a stronger affinity for an octahedral site than does Fe^{3+} so $(Fe^{3+})[M^{2+}Fe^{3+}]$. As per popular convention, ions in parentheses represent those on tetrahedral sites and those in brackets occupy octahedral sites. All cations have 4 or 6 oxygen ions as nearest-neighbors depending on tetrahedral or octahedral occupation. While it is widely known that the selection of a preferential lattice site is largely dependent on the ionic radius of M^{2+}, the intention here is to investigate this preference as a function of ion concentration in solution chemical syntheses.

1.4 Chemical Synthesis of Ferrite Nanoparticles

Several methods have been explored to synthesize cobalt ferrite nanoparticles including chemical reactions in water-in-oil emulsions,[15] sol-gel chemistry,[16] and templated assembly.[17] Here, we modify the coprecipitation method of Caruntu, et.al,[18,19] and exclude the addition of any long-chain hydrocarbon capping ligand during synthesis. A series of six samples of $Co_xFe_{1-x}Fe_2O_4$

nanoparticles has been produced, where $0 \leq x \leq 1$. Structural, magnetic, and magneto-optical properties of these materials have been studied which, collectively, allow the qualitative determination of the composition of the products. Analysis of the key electronic transitions responsible for the magneto-optical response leads to the conclusion that the product is one homogeneous spinel product, for all x, with three type of cations (Co^{2+}, Fe^{2+}, Fe^{3+}) in an octahedral field with both Co^{2+} and Fe^{3+} occupying the tetrahedral sites and not simply a physical mixture of $CoFe_2O_4$ and Fe_3O_4.

CHAPTER 2-THEORY

2.1 Maxwell's Equations

While the Faraday effect is the object of the current discussion, all magneto-optical effects are the product of an electromagnetic (EM) wave interacting with some sample and, as such, the nature of these interactions must be established. Faraday rotation is defined as the rotation of the plane of polarization of incident as it passes through a sample. The sample engaged exhibits two different indices of refraction, η_1 and η_2, corresponding to different responses to the incoming light. This property of a material is generally known as birefringence, meaning two refractions, or dichroism more specifically.[20] Birefringence refers to all materials that have two responses to some type of incoming radiation while dichroism refers to differing optical properties for incoming light of different polarizations. This study deals with *magnetic circular dichroism*, whereby a material exhibits a different optical response to the two different optical circular polarization states. In general, a single-wavelength incident polarized beam of light can be equivalently described as the superposition of two linear or two circular polarization states. These polarization states are referred to as right-handed circularly polarized light (RCP) and left-handed circularly polarized light (LCP) where the electric field vector rotations clockwise for RCP and counterclockwise for LCP, when viewed toward the source as depicted in Fig. 2.1.

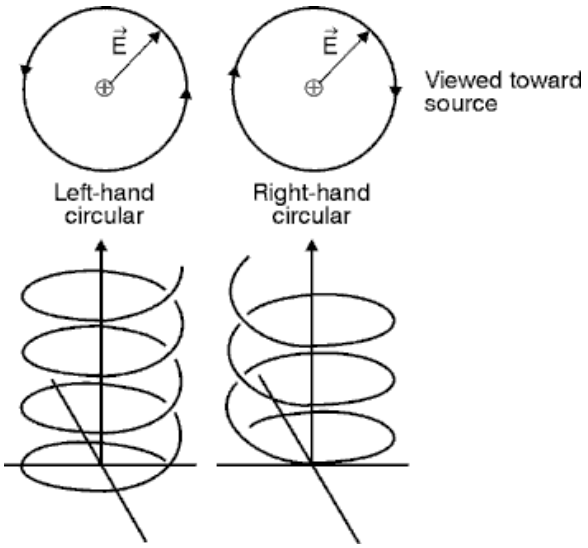

Figure 2.1 Electric field vector of left- and right- circularly polarized light.

Faraday rotation, a result of magnetic circular dichroism, is the difference between the response of the material to RCP and LCP. These responses may be taken to be the right-handed index of refraction (η_+) and the left-handed index of refraction (η_-). Before proceeding further, the relationships between Maxwell's equations and the indices of refraction must now be established. It must be noted here that the experiment is set up in the polar configuration so that the magnetic field lines are in the same direction as the optic axis, taken to be the *z*-axis. The optic axis simply refers to direction of propagation of the incident and will be referred to as the propagation vector, **k**. from now on. An optical electromagnetic field, being transverse, would be polarized in the *x*-*y* plane. Maxwell's very famous equations, listed below, are the most obvious place to begin the description of this interaction and the results thereof. With no sources, in a medium, Maxwell's equations are[21]

$$\nabla \cdot \mathbf{D} = 0 \text{ (Gauss's Law)} \tag{2.1}$$

$$\nabla \cdot \mathbf{B} = 0 \text{ (Gauss's Law-Magnetic)} \tag{2.2}$$

$$\nabla \times \mathbf{E} = -\partial \mathbf{B}/\partial t \quad \text{(Faraday's Law)} \tag{2.3}$$

$$\nabla \times \mathbf{H} = \mu \partial \mathbf{D}/\partial t \quad \text{(Ampere's Induction Law)} \tag{2.4}$$

where **D** is the electric field displacement vector and corresponds to the electric field due to any free charges in the sample and **E** is the applied electric field.

$$\mathbf{D} = \varepsilon_0(\mathbf{E} + \mathbf{P}) \tag{2.5}$$

with **P** representing the electric field produced by any electric dipoles in the sample. **B** is the magnetic flux density vector and is related to **H**, the magnetic field vector, by

$$\mathbf{B} = \mu_0(\mathbf{H} + \mathbf{M}) \tag{2.6}$$

where **M** (magnetization or the magnetic moment per unit volume) is the magnetic field produced by the sample. For ferromagnets and paramagnets, H and **M** are in the same direction while their signs differ for diamagnets as a result of their opposition to the applied field.

In any medium, the response of a material to the electric field is described by the electric permittivity, ε. In a magneto-optically active medium, the constitutive relation between the electric field and displacement field,[2]

$$\mathbf{D} = \bar{\bar{\varepsilon}}\mathbf{E}\,. \tag{2.7}$$

where $\bar{\bar{\varepsilon}}$ is the complex permittivity tensor which includes the magneto-optical (gyrotropic) response,[2]

$$\bar{\bar{\varepsilon}} = \begin{bmatrix} \tilde{\varepsilon}_1 & -ig & 0 \\ ig & \tilde{\varepsilon}_1 & 0 \\ 0 & 0 & \tilde{\varepsilon}_0 \end{bmatrix}, \tag{2.8}$$

where $\tilde{\varepsilon}_1 \approx \tilde{\varepsilon}_0$ is the linear response. The magneto-optical response is defined by the gyration vector, g, which to the first approximation depends linearly on the magnetization, $\mathbf{M}$.[2] Here, only the *z* component of this vector is shown. The gyration vector and the permittivity tensor of a magneto-optical sample are often written in terms of the Voigt parameter, Q with[2]

$$g / \varepsilon_1 = Q = Q' + iQ'' \tag{2.9}$$

Notice that the Voigt parameter takes into account the real and imaginary parts of transmittance, including absorption. The permittivity tensor now includes all aspects of the material.

Maxwell's equations, (2.3) and (2.4) can be combined to yield a wave equation for the electric field, $\mathbf{E}$

$$-\nabla^2\mathbf{E} + \nabla(\nabla\cdot\mathbf{E}) = -\mu_0 \frac{\partial^2\mathbf{D}}{\partial t^2} \tag{2.10}$$

At optical frequencies, the relative permeability is 1, so that μ_0 is used in the equation.[22] The solution for a plane wave travelling in the *z* direction is given by

$$\mathbf{E} = \mathbf{E_0} e^{i(\mathbf{k}\cdot\mathbf{r}-\omega t)}. \tag{2.11}$$

Substituting this into the wave equation yields,

$$-k^2\mathbf{E} + \mathbf{k}(\mathbf{k}\cdot\mathbf{E}) = -\omega^2\mu_0\bar{\bar{\varepsilon}}\mathbf{E} \tag{2.12}$$

Assuming propagation along the *z* axis so that $\mathbf{k} = k\,\hat{\mathbf{e}}_z$, this equation has a non-trivial solution only if the determinant of the coefficients vanishes or

$$\eta_\pm{}^2 = \frac{c^2}{\omega^2}k^2 = \varepsilon_1 \pm g = \varepsilon_1\left(1 \pm Q\right). \tag{2.13}$$

The normal modes of propagation are now identified as right- and left- circular polarizations described by the indices of refraction, $\eta_\pm$. These indices can be written

$$\eta_+ = \varepsilon_0\mu_0(1 + Q) \text{ and } \eta_- = \varepsilon_0\mu_0(1 - Q) \tag{2.14}$$

An expression for the complex Faraday rotation is be derived dependent on the difference between η_+ and η_-, the incoming wave frequency, ω, and the Voigt parameter.

$$\theta_F = \frac{\pi}{\lambda}\frac{g}{\sqrt{\varepsilon_1}} = \frac{\pi}{\lambda}(\eta_+ - \eta_-)Q \tag{2.15}$$

where the real part is generally referred to as the Faraday rotation and the imaginary part is referred to as the Faraday ellipticity.

2.2 Permittivity Tensor

Recalling that Faraday rotation is the result of two indices, the origin of these two indices is now discussed. Magnetization occurs in a sample (in an applied magnetic field) as a collective response from the electrons in the sample to the magnetic field. Depending on the orientation of a given electron, this response will be different. Electrons that occupy the same orbital differ only in the orientation of their spin. Therefore, they will respond to an applied field in exactly the opposite manner. Additionally, if all electrons in a sample are paired, the net magnetization of the sample will be zero. In the case of some metal cations, there are some unpaired electrons with parallel spins, leading to an overall magnetization. These unpaired electrons and their response to a magnetic field are the subject of the next section as they are the key to a semi-classical understanding the magneto-optical effect.

The Lorentz force is the force on a charged particle by a magnetic field and as such will be felt by electrons under $\mathbf{B}_{app}$ resulting in a distorted electron cloud.[23] If the motion of free electrons without $\mathbf{B}_{app}$ is taken to be the combination of two types of circular motion (modes) within its orbital, one clockwise and one counterclockwise, then both of these modes are represented by its

normal motion and no effect is observed. With the Lorentz force taken into account, the orbit of the electron distorted, the motion of these modes will no longer be equal. In fact, it the difference in the response of these circular modes which result in a magnetic circular dichroism -- since distortion of the electron cloud is proportional to the $\mathbf{B}_{app}$, it seems quite reasonable that the Faraday effect is also dependent on $\mathbf{B}_{app}$. This behavior is known as induced gyrotropy and is responsible for all magneto-optical effects. The spins of unpaired electrons in the sublattices of ferrites align parallel to each other and oscillate right-handed or left-handed accordingly based on the cation to which they belong. The precession of these electrons may be defined by the gyration vector, $\mathbf{g}$, which just describes an electron's movement in a given direction. While some materials are naturally birefringent to a small degree, the application of magnetic field greatly increases the anisotropy of the magnetizable material.[2,23]

From Maxwell's equations, it is possible to obtain an expression for the magnitude of *k* in terms of the material's response to E (permittivity,ε) and B (permeability,μ). These quantities collectively determine the speed and phase of an incident EM wave, with frequency,ω, propagates through the material.

$$k = \frac{\omega}{c}\sqrt{\varepsilon\mu} = \frac{\omega}{c}\eta\,, \tag{2.16}$$

where η is the linear index of refraction (g=0) and the material parameters are generally complex.

This expression merely says that the propagation of an EM wave through a medium is dependent on both the frequency of the incoming wave, ω and the material response, ε and μ. The real parts of this tensor results from normal dispersion through the medium of interest while

the imaginary parts account for energy lost during propagation.[5] In all cases, the processes result from electronic transitions and vibronic excitations. As our intention here is not to quantify any part of the dielectric tensor for these samples, it will suffice to say here that the magneto-optical spectra discussed presently are the result of both normal dispersion and absorption.

2.3 Electronic Transitions in Ferrites

The Voigt parameter is the primary parameter in the determination of Faraday rotation. The reasons for a given measured value of the Voigt parameter are still difficult to quantify. The values of each part of the gyration and permittivity vectors are different corresponding to different absorption coefficients for different orientations of an impinging EM wave. These differences result in a Faraday rotation spectrum that fluctuates according to these values at a given wavelength. Based on the changes in the Faraday spectrum, it must be concluded that something is changing inside the material as the wavelength changes. As it has been shown that this phenomenon is largely dependent on the state of the orbital that an unpaired electron occupies,[23] there are two possibilities for a frequency-dependent Faraday spectrum: 1) the response to the magnetic (Lorentz) force on the electronic orbital is heavily-dependent on wavelength (frequency) or 2) the electron has made a transition to a different orbital. While option 1) may at first seem to be the source, the applied field is constant and the electron cloud will not change much as a result of **B** from the wave, so the electron must have relocated to a new orbital. While possible locations of this new orbital may seem endless, selection rules may be applied to reduce these possibilities.

Intervalence Charge Transition

An intervalence charge transfer transition (IVCT) can be viewed as the short-term electron transfer between two different cations in a lattice.[24-26] Envision two cations on different lattices in a structural and give an unpaired electron one of them a restoring force, ω_0. Now, there is some distance (lattice parameter) that separates the electron clouds of these two cations. The electron, with ω_0, oscillates around its mean axis according to its gyration vector and reaches its maximum displacement from the axis at some frequency, ω. This displacement is given by

$$\mathbf{r} = \frac{e\mathbf{E}}{m_e\left(\omega_0^2 - \omega^2\right)} \tag{2.17}$$

If the maximum displacement of the electron is in the domain of another cation, the electron has been promoted to that cation, if only for a short time.

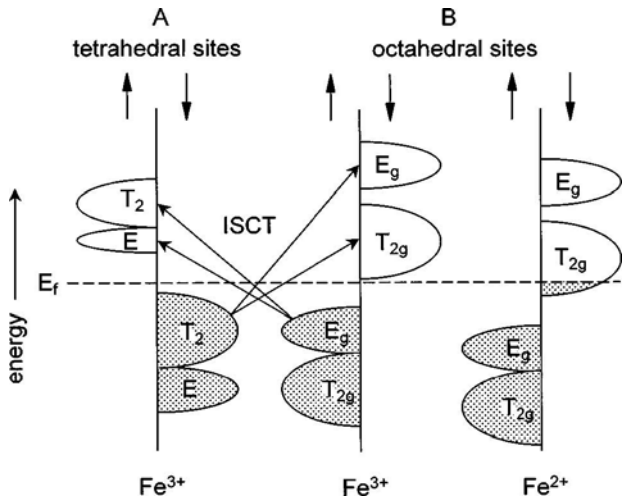

Figure 2.2 Proposed electronic energy levels and transitions in magnetite.[26]

The electron will likely return to its original energy level very quickly, around 1 ps,[27] and the process begins again when incoming EM energy promotes it. This repeated promotion and relaxation of electrons are Drude-like oscillations and result in the electron being in a different orbital on a different cation at the proper wavelength, while under an applied magnetic field.

$$M^{2+} + Fe^{3+} \Leftrightarrow M^{3+} + Fe^{2+} \tag{2.18}$$

As these transitions involve two metals, they are partially allowed *d*-orbital transitions where the lattice sites in question are the tetrahedral and octahedral sublattices. *d-d* transitions are responsible for the color in certain gems and occur as a result of impurities in the crystal lattice. For example, in the case of sapphire,[28] an electron is promoted from titanium to iron and back,

$$Fe^{2+} + Ti^{4+} \Leftrightarrow Fe^{3+} + Ti^{3+} \tag{2.19}$$

If the energy levels of the *d*-orbitals for each cation are known, IVCT transition identifications can be made from changes in magneto-optical spectra. While *d-d* transitions are somewhat forbidden, the transitions discussed presently are facilitated by *p*-orbitals from neighboring oxygen atoms so that the effective transition route is *d-p-d*.

Other transitions

IVCT transitions are not the only processes initiated by the absorption of EM energy, however. An IVCT that occurs between like cations on different sublattices constitutes an intersublattice

charge transfer (ISCT) transition. ISCT transitions are generally lower in energy than their counterpart due to the same type of cations being involved.

$$2Fe^{3+} \Leftrightarrow Fe^{2+} + Fe^{4+} \qquad (2.20)$$

In the case of magnetite, Fe^{2+} is low spin and has a stronger affinity for octahdedral coordination than does Fe^{3+}, so Fe^{2+} occupies half of the octahedral sites while Fe^{3+} occupies the other half as well as all the tetrahedral sights. Crystal field-diagrams for octahedral Fe^{2+} and tetrahedral Fe^{3+} are shown below.

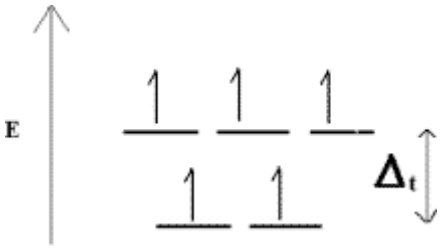

Fig. 2.3a CF Diagram for tetrahedral Fe^{3+}

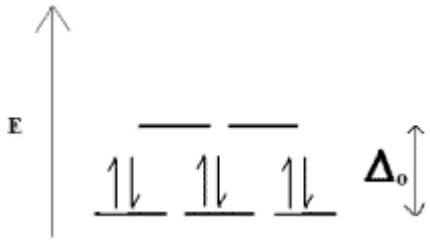

Fig. 2.3b CF Diagram for octahedral Fe^{2+}

While Fe^{4+} is certainly not the most common oxidation state of iron, it is known to coexist, albeit in very small amounts, with Fe^{2+} in nearly all garnets.[4]

The last process to be discussed here is the crystal field transition (CF). A CF transition is simply the promotion of an electron from one energy level to another in its own electron cloud. While it may seem that numerous of these CF transitions occur, the selection rules for them limits the number of allowed transitions. First, CF transitions in an octahedrally coordinated compound are mostly forbidden due to the inversion symmetry associated with it being surrounded by six identical oxygen anions. However, CF transitions in an octahedral cation are

slightly allowed if some impurities are introduced and the symmetry is significantly reduced. Transitions that alter the number of unpaired electrons in a given shell are also forbidden. Based on these selection rules, CF transitions in magneto-optical samples are only allowed for tetrahedral coordination where these transitions are limited even further by the unpaired electron rule. The energy of CF transitions in tetrahedral coordination versus octahedral coordination is naturally much lower based on larger field splitting, dq, for an octahedron.[13] An example CF transition is shown in Fig. 2.4 below.

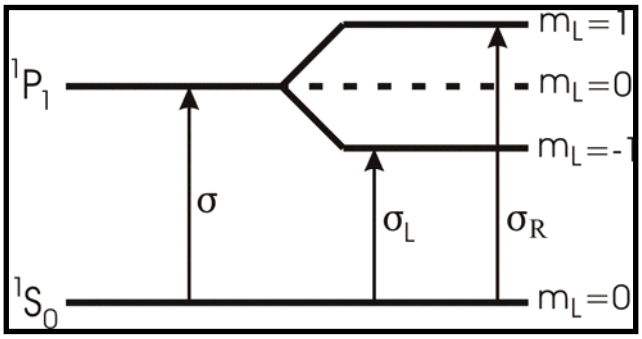

Figure 2.4 Zeeman splitting and corresponding allowed CF transitions for a given material.[13]

The diagram above is that of set of generic CF transitions in a magnified sample. The ground state of the electrons involved in this transition remains degenerate while the excited P-state undergoes Zeeman splitting in the presence of the applied magnetic field. Any allowed transitions must have $\Delta l = \pm 1$. Zeeman splitting may be viewed as further crystal splitting of the originally degenerate orbitals in response to an applied magnetic field. The *d*-orbitals of an isolated transition metal ion in a vacuum display 5-fold degeneracy until placed in a crystal lattice where the splitting of these orbitals is the necessary response of the orbitals to Coulomb interactions with the rest of the lattice. Once situated in its preferential lattice site in a ccp structure, the ground state will either be triply or doubly degenerate, depending on octahedral or

tetrahedral coordination (See Fig. 2.3). The degenerate excited state here is split into 3 non-degenerate states when under a magnetic field where only two of these, $m_l = \pm 1$, will facilitate an allowed CF transition.

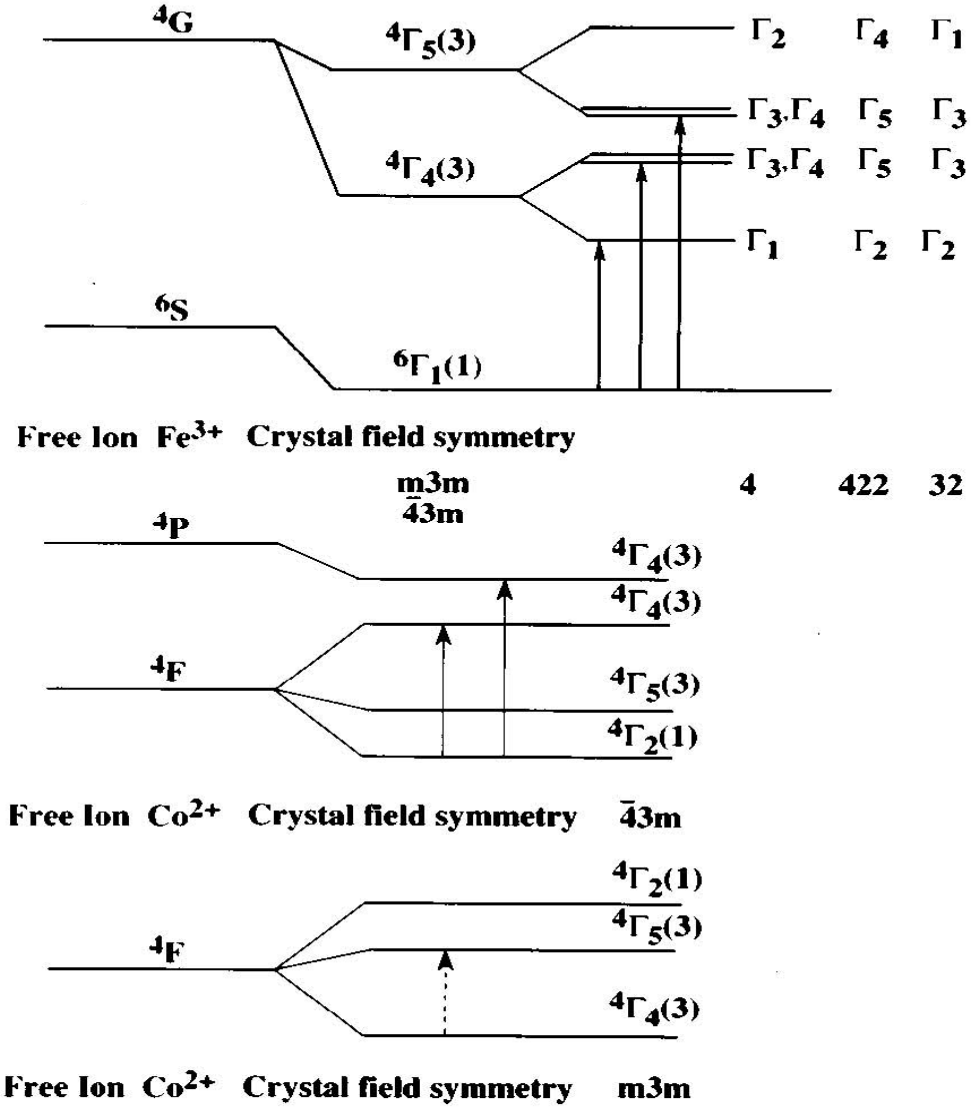

Fig. 2.5 CF transitions for octahedral Fe^{3+} and Co^{2+}. Transitions for Co^{2+} are also shown.[35]

CHAPTER 3 - EXPERIMENT

3.1 Chemical Synthesis

As a series with differing divalent characters is the object of this study, all products were synthesized by a co-precipitation method based on Caruntu et.al.,[18,19] which yields homogeneous, spherical ferrite nanoparticles. Based on previous studies, the magneto-optical response of a nanoscale material is dependent on the shape of the particles in the sample.[8,29] Therefore, a homogeneous sample is paramount, as a sample containing particles of different shapes exhibits a combination of anisotropy constants resulting in a much more complicated magneto-optical spectrum. While not the largest rotators of circularly polarized light, a series of ferrites was chosen over garnets, which display the largest known θ_F, due to the amount of control during the synthesis. Attempts with garnets, namely yttrium-iron-garnet ($Y_3Fe_5O_{12}$), can only be described as moderately successful as the morphology of the products was inhomogeneous and the average grain size was > 200 nm, beyond the nanoscale scope of this project.

$Co_xFe_{1-x}Fe_2O_4$ fine powders were synthesized based on the coprecipitation mentioned above but without the addition of any capping ligand so as to provide more options for substrates and background matrices. All starting materials were purchased from Sigma-Aldrich Co. and used as is, with no further purification. Approximately 640 mg of sodium hydroxide, NaOH, pellets were dissolved in 40 ml diethylene glycol, or DEG, at ~80°C overnight in a sealed 150 ml bottle.

DEG was chosen as the solvent because it is a high boiling polar solvent which allows not only for the reactions to take place at higher temperatures but also for the precipitate to fall out at a much slower pace. The rate at which a nanoscale reaction cools seems to be a very important factor as to the size and shape of the product where rapid cooling can lead to inconsistencies in the characteristics of the product. As fluctuations in temperature during product formation also affect morphology, a digital temperature controller monitored all reactions in order to minimize these effects. While DEG is a very suitable solvent for this reaction, it cannot facilitate the entire process without the aid of some water. The presence of some small amount of water was the motivation for choosing hydrates ($FeCl_2 \cdot 4H_2O$, $FeCl_3 \cdot 6H_2O$, $CoCl_2 \cdot 6H_2O$) as starting materials over their anhydrous counterparts. The proposed mechanism for this reaction is given below.[19]

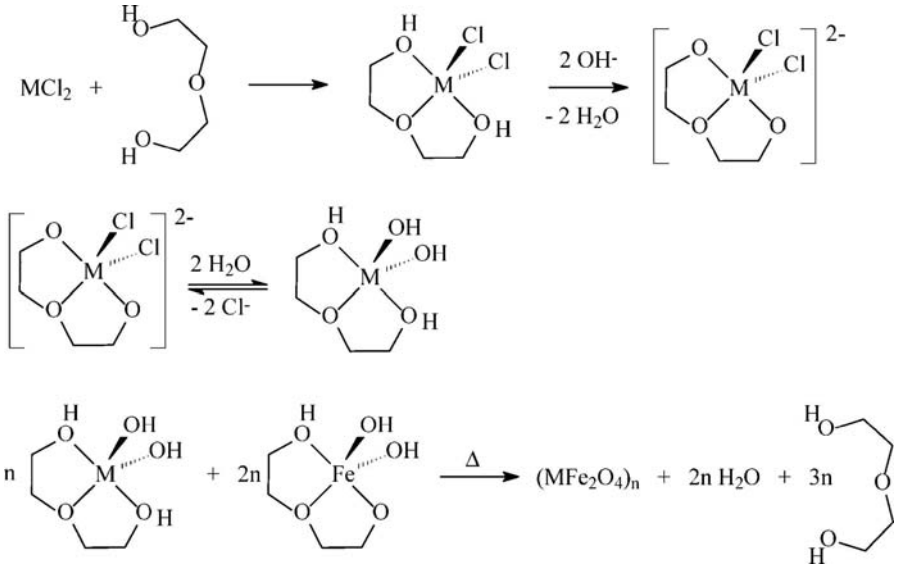

Figure 3.1 Proposed chemical reaction for producing inorganic ferrites from iron chloride salts.[19]

Based on this mechanism, DEG is essential in that it forms quite stable intermediate complexes with the metal cations involved in this reaction. These complexes are then hydrolyzed resulting in the removal of all chloride species, which gives the proper chelated hydroxide of each metal.

In a separate vessel from the previously mentioned NaOH-DEG solution, a solution of the metal chloride hydrates was prepared in a 125 ml round-bottomed 4-neck flask. All reactions proceeded in this manner with the only notable variable being the concentrations of the divalent chlorides where y mmol of $FeCl_2 \cdot 4H_2O$, z mmol of $CoCl_2 \cdot 6H_2O$ (where $y + z = 2$ mmol) and 4 mmol $FeCl_3 \cdot 6H_2O$ were dissolved in 40 ml DEG at room temperature under argon. Table I contains the corresponding values for all values of x.

Table I. Precursor quantities for cobalt ferrite synthesis

	Metal salt amount (mg)		
Cobalt mole ratio, x	$CoCl_2 \cdot 6H_2O$	$FeCl_2 \cdot 4H_2O$	$FeCl_3 \cdot 6H_2O$
0	0.0	397.0	1081.0
0.2	95.2	317.5	1081.0
0.4	190.4	238.0	1081.0
0.6	285.5	158.5	1081.0
0.8	380.7	79.5	1081.0
1.0	475.9	0.0	1081.0

The warm NaOH/DEG solution was added to the metal chlorides in DEG and an immediate color change took place. This color change corresponds to the formation of $Fe(OH)_2$, $Co(OH)_2$, and $Fe(OH)_3$, respectively, but does not indicate anything regarding the target products. The hydroxides are, in fact, chelated by a DEG anion that must be removed in order for the metal oxides to form. Once the hydroxides formed, the reaction flask was slowly heated to 215°C over 90 minutes and allowed to continue at this temperature for an additional 30 minutes. Increasing the temperature of the environment of the hydroxides initiates further hydrolysis resulting in the formation of the sought after metal oxides. The reaction flask was allowed to cool very slowly and the products were collected and washed repeatedly with methanol to remove any unwanted

reagents or solvent still bound to the particles. Following a methanol wash, the products were centrifuged at 5000 RPM for 20 min and the supernatant decanted. Each sample was washed and centrifuged three times, then dried and collected for further study.

3.2 Structural Analysis

As is generally the case in determining the complete structure of a given material, several techniques are applied here so as to piece together the true identity of these newly synthesized products. Given the nanoscale scope of this study, a transmission electron microscopy, or TEM, image of the product must be obtained to confirm that the product is comprised of homogeneous, crystalline nanoparticles. In case of an inhomogeneous or amorphous sample, the product must be discarded and the synthesis repeated or even altered. Solutions for TEM observation of the products were prepared by stabilizing the particles with 1M-tetramethyl ammonium hydroxide, TM-NH_4OH, and suspending them in water. A drop of the aqueous solution was placed on a carbon grid and heated to ~60° C overnight to remove any excess water from the grid. TEM images were obtained from A JEOL-2010 Supertwin TEM at 200 kV. The JEOL-2010 is also equipped with energy dispersive x-ray spectroscopy (EDS) that allows for the determination of the elemental distribution in the sample. This determination is accomplished by analyzing the energy of x-rays emitted from the sample upon absorption of incoming energy from the electron beam.[30] As the energy of the x-ray is characteristic of the electronic energy level from which it was emitted, the source element may be calculated and its concentration found relative to any other constituents. Because this technique is much more reliable for metals and heavier elements than for lighter ones, EDS is not reliable for the oxygen content in any sample, thus oxygen content will not be reported.[30]

Dried powders of each sample were placed in a PANalytical X'Pert Pro diffractometer and x-ray diffraction (XRD) patterns of all samples were established from $20° \leq 2\theta \leq 75°$. XRD patterns give not only the type of crystal lattice the product but also some insight into the degree of crystallinity. Application of the Debye-Scherrer equation to an XRD pattern provides the theoretical average grain size and is given by:[13]

$$d = \frac{0.9\lambda}{\delta \cos(\theta)}, \tag{3.1}$$

where λ is the x-ray wavelength, δ is the full-width at half maximum of the x-ray peak at the angle θ.

Magnetic properties (magnetization) were measured on a Vector VSM at room temperature for all values of *x*. A VSM, or vibrating sample magnetometer, is a device by which the magnetic moment of a sample may be determined quite easily over a large range of magnetic field strengths.[4] While the VSM returns the total magnetic moment from a material, the moment per unit mass, μ/m, is characteristic of the type of sample and may be used to further understand the structural properties of an unidentified material. As a change in magnetic behavior obviously is a result of corresponding structural and compositional changes, trends in magnetic data as a function of some varying parameter may aid in the identification of that parameter's preferences, adding significant insight into the reasons behind the system in question. 50 mg of dried $Co_xFe_{1-x}Fe_2O_4$ powder was inserted into the sample holder where the total magnetic moment of each sample was measured from -10000 G to 10000 G.

3.3 Magneto-Optical Setup

The gathering of magnetic data from magnetic circular dichroism MCD is more complicated than the previous techniques as cheaper commercial instruments are available for VSM, XRD, and TEM. The experimental setup will be established here (Figure 3.2) followed first by a account of sample preparation for optical measurements.

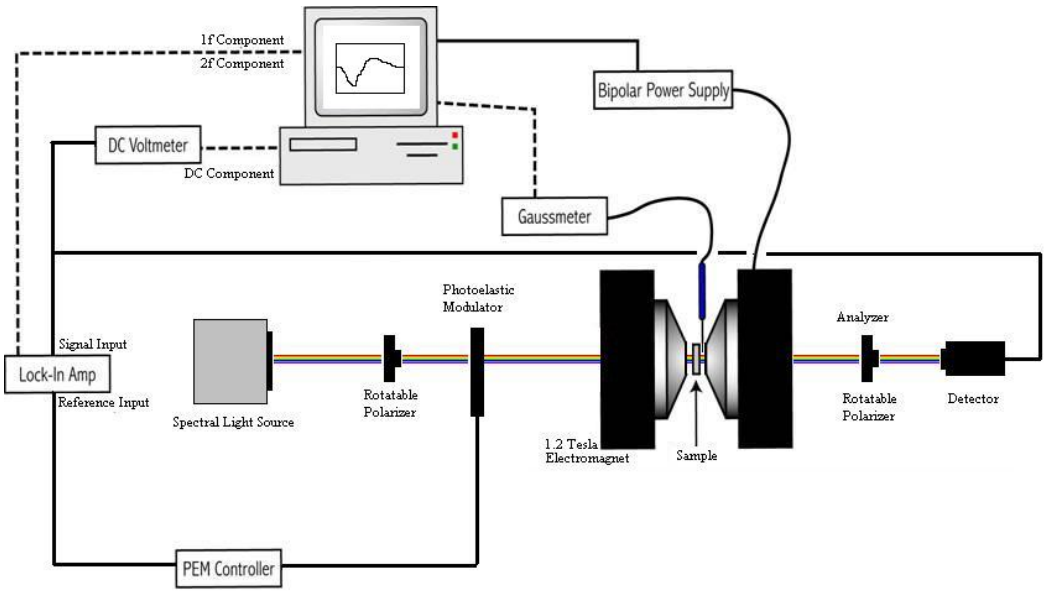

Fig 3.2 Magneto-optical spectrometer

Spectral Faraday rotation measurements were made by the photoelastic modulator technique.[29] As the name implies, a photoelastic modulator (PEM) is used here to produce polarized light that cycles from RCP to LCP and back again. The photoelastic modulator acts as a quarter-wave plate whereby one component of incoming linear polarized light is given a phase lag (ε) of $\pi/2$. The phase difference translates into RCP or LCP depending on which component of the incident EM wave is retarded by $\pi/2$. RCP ($+\pi/2$) corresponds to lagging E_y and, likewise, LCP ($-\pi/2$) with E_x trailing by a quarter wave.[20]

Table II. Summary of plane-wave electromagnetic field components for polarized light.[20]

Linearly Polarized (LP)	Right circularly polarized (RCP)	Left circularly polarized (LCP)
$\mathbf{E}_x = \mathbf{E}_y = \mathbf{E}_0 \cos(kz - \omega t)$	$\mathbf{E}_x = \mathbf{E}_{0x} \cos(kz - \omega t)$	$\mathbf{E}_x = \mathbf{E}_{0x} \cos(kz - \omega t)$
	$\mathbf{E}_y = \mathbf{E}_{0y} \cos(kz - \omega t + \pi/2)$	$\mathbf{E}_y = \mathbf{E}_{0y} \cos(kz - \omega t + \pi/2)$

Having established these extreme states of the incident disturbance, it must be noted that not all the incident radiation is purely RCP or LCP. The modulator changes the phase of the polarization along the axis of retardation sinusoidally at a frequency of 50 kHz resulting in a beam that rotates through several polarization states, with $-\pi/2 \leq \varepsilon \leq \pi/2$, as seen in Figure 3.3.

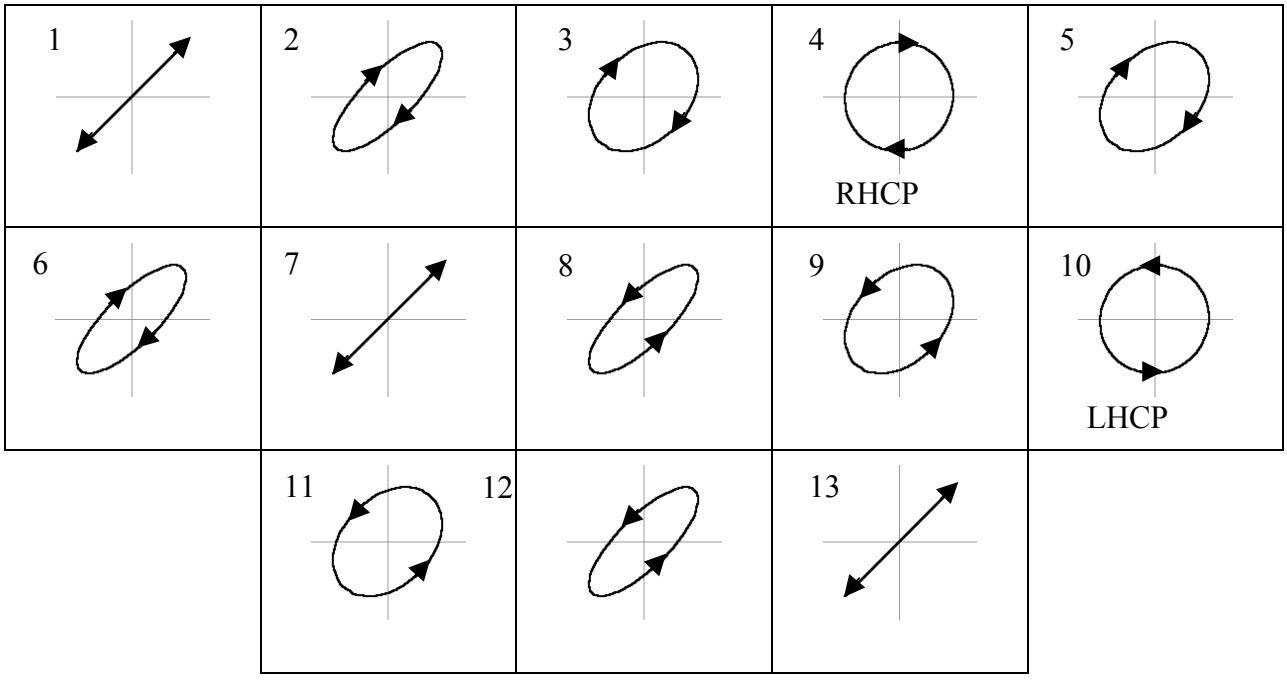

Figure 3.3 Linearly polarized light modulated by the photoelastic alternates between right- and left-circularly polarized at a frequency of about 50 kHz.[31]

The source of E_x and E_y is a 100 W halogen lamp capable of producing natural light with frequencies from 400-1000 nm. The natural light is then wavelength dispersed by a 0.3-m monochromator that selects 400 nm as the first wavelength and increases by increments of 5 nm to the following wavelength until 1000 nm is reached. After a particular wavelength has been selected and the beam linearly polarized, the LP-state beam passes through the PEM and impinges on the sample under its current conditions. Ferrofluids of each sample in this series were prepared by suspending approximately 2 mg of dried powder in 1 mL of 1 M $TMNH_4OH$ (aq) and 2 mL of deionized water. A few drops of these solutions (~50 μL) were placed on silica substrates and dried overnight at approximately 40°C. The resulting films were then placed between the poles of an electromagnet with the magnetization parallel to the propagation of light (polar configuration) where the applied magnetic field was 4000 G. The end result of the entire setup is a beam of alternating circular polarization impinging on a sample that is magnetized by a known applied magnetic force. The beam passes through the sample and on to a silicon avalanche photodiode connected to a lock-in amplifier referenced to the PEM. In this way, the lock-in directly measures the difference in index of refraction between right and left circularly polarized light. The data is averaged data over the entire range of polarization states three times before returning the difference in η_R and η_L. The difference between the indices for RCP and LCP, $(\eta_R - \eta_L)$, is the effective Faraday rotation at a given wavelength as is reported in Fig 4.4.

CHAPTER 4- RESULTS

4.1 Structural Analysis

Transmission Electron Microscopy

TEM observations confirm the presence of 5-8 nm particles exclusively for all studied values of x, and EDS analysis confirms the correct Fe/Co ratio for all samples. A representative TEM image is shown in Figure 4.1. A comparative scale is shown on the left.

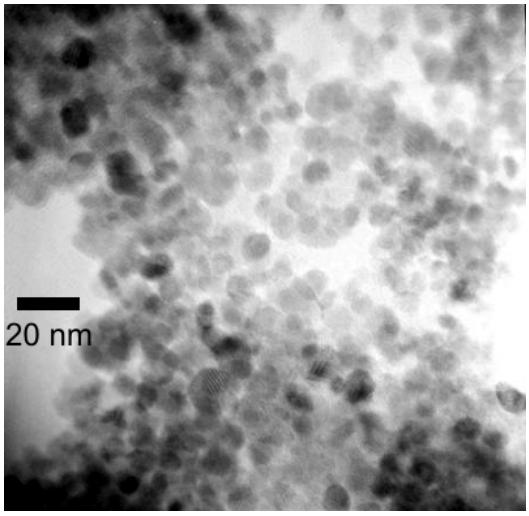

Figure 4.1 Transmission electron microscope image of Fe_3O_4 (x=0) nanoparticles.

X-ray Diffraction

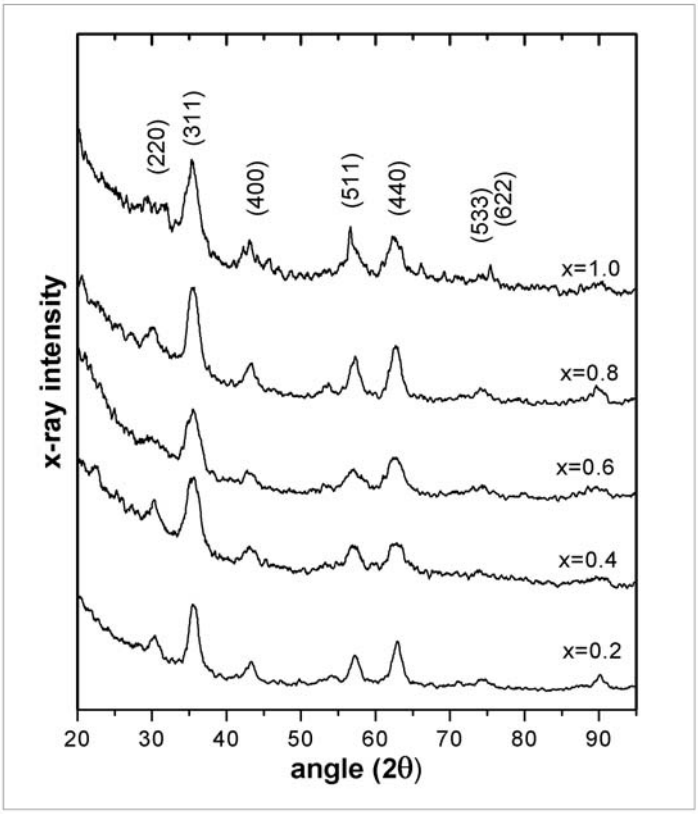

Fig. 4.2 X-ray diffraction patterns for $Co_xFe_{1-x}Fe_2O_4$

X-ray diffraction patterns are shown in Figure 2 for the complete data series. The angle of the incident Cu-K_α radiation is varied from 20° to 75° for all samples. The entire series returns consistent diffraction patterns with some slight variations to be discussed in the next chapter.

Magnetization

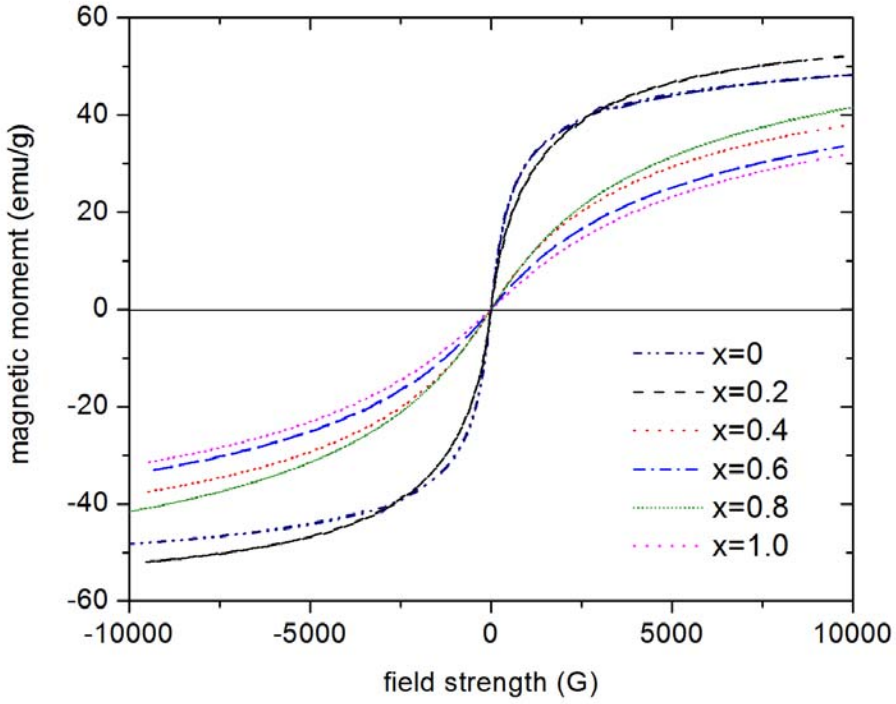

Figure 4.3 Magnetization data for the cobalt ferrite nanoparticles.

Magnetic data (magnetization v. applied magnetic field) is shown in Figure 4.3. The total magnetic moment is measured for each sample from -10000 G to 10000 G. This maximum field of our vibrating sample magnetometer (10,000 G or 1 T) is insufficient to saturate the magnetization. In all cases, the nanoparticles are expected to be superparamagnetic. The magnetization and susceptibility of superparamagnetic particles can be modeled using the formalism for classical bulk paramagnets by replacing the atomic moments the moment of the nanoparticle.[32] The magnetic moment of a sample containing *N* interacting particles is given by[4,32]

$$m(H) = Nm_0\left[\coth\left(\frac{m_0\mu_0 H}{k_B T}\right) - \frac{k_B T}{m_0\mu_0 H}\right] \tag{4.1}$$

where m_0 is the magnetic moment of the particle, k_B is the Boltzmann constant, T is the absolute temperature and H is the applied magnetic field. The magnetic moment of the each individual particle is $m_0 = M_S V_0$, where M_S is the bulk saturation magnetization and V_P is the particle volume. Literature values for the bulk parameters for Fe_3O_4 and $CoFe_2O_4$ are given in Table II.

Table II. Bulk physical and magnetic parameters for magnetite and cobalt ferrite.[3,33]

	saturation magnetization (emu/g)	density (g/cm^3)	particle volume (cm^3)	magnetic moment (A/m)
Fe_3O_4	92.0	5.193	1.13×10^{-19}	1.28×10^{-13}
$CoFe_2O_4$	75.0	5.294	1.13×10^{-19}	1.06×10^{-13}

Using the expansion of coth()

$$\coth(x) = \frac{1}{x} + \frac{x}{3} - \frac{x^3}{45} + \ldots \tag{4.2}$$

so that for low fields with $x = m_0 H / k_B T$,

$$\frac{m(H)}{Nm_0} \approx \frac{1}{3}\frac{m_0 H}{k_B T} \tag{4.3}$$

The slope of $M(H)$ v. H (low field susceptibility) is $\chi \approx \frac{N}{3}\frac{m_0^2}{k_B T}$. We can, therefore, make some statements about the intrinsic saturation magnetization of the sample by examining the initial susceptibility or the slope of magnetization v. applied field at low fields. We do observe the expected trend of systematically decreasing saturation magnetization with increasing *x*, with the exception of *x*=0.8 which will be addressed in the discussion section.

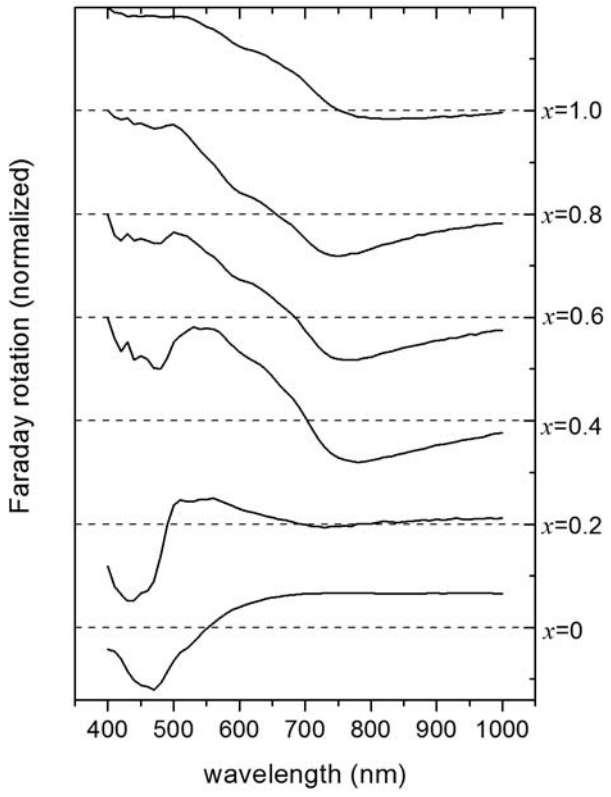

Figure 4.4 Faraday rotation spectra for the $Co_xFe_{1-x}Fe_2O_4$ nanoparticles. The spectra are offset for clarity; the value for *x* on the right hand side is next to the zero for that spectra.

Magneto-optical spectra for all values of *x* from 400-1000 nm are displayed. Several aspects of the spectra are noteworthy: 1) A change in the direction of Faraday rotation as increases from 400-500 nm, 2) The emergence and subsequent disappearance of broad peak centered around 550 nm, 3) A noticeable shoulder around 625 nm as *x* increases, and 4) a minimum at approximately 750 nm.

CHAPTER 5 - DISCUSSION

TEM, XRD, and VSM

Application of the Debye-Scherrer equation returns an average grain size in these samples of 3 nm but TEM observations indicate that the mean particle size is actually closer to 8 nm. Although this may seem to be inconsequential, this value is more than 100% larger than the theoretical particle size. Patterns from all samples index to a spinel-group structure, but the type of spinel for each is indiscernible here as the sizes of the divalent cations in this system are nearly identical, Co^{2+} = 65 pm and Fe^{2+} = 61 pm.[34] Indexing an XRD pattern gives the spatial arrangement of the species in a unit cell with respect to each other but no information concerning the identity of those species. Normally, this information is not a problem as the structure of the sample in question may be pinpointed based solely on concentrations of components and the d-spacings between each one. In this case, tetrahedral and octahedral coordination for Fe^{2+} instead of Co^{2+} cannot be determined from this series of diffraction patterns as they merely confirm that some ion with a radius of ~ 60 pm is located ~8.4 Å from a similarly-sized cation.[35] While all samples are indeed spinels, the pattern for x=0.6 returns much broader peaks with lower intensities than the rest of the series. As this peak broadening does not arise from smaller than expected particle sizes, inconsistencies in the crystal lattice or decreased crystallinity is the likely cause.

Moving onto VSM data, the behavior of the series is as predicted, based on the superparamagnetic properties of cobalt ferrite nanoparticles smaller than ~20 nm,[36] and provides further evidence of the incorporation of Co^{2+} into the final product. Noticeably, the magnetic moment of $x = 0.6$ is less than for x = 0.8. It is expected that fewer Fe^{2+} and more Co^{2+} will result in a smaller magnetic moment due to Co^{2+} having fewer unpaired electrons than Fe^{2+}. The magnetic moment per unit mass for this series ranges from ±30-50 emu/g at ±10000 G where the smallest moment occurs when $x = 1$. The jump by the x= 0.8 may be viewed as evidence for more low-spin octahedral Co^{2+} than for $x = 0.6$. This shift in the octahedral component is most likely due to some fluctuation in the argon flow during synthesis.[35]

Analysis of the magneto-optical spectra of thin films of these samples gives us the strongest insight into the properties of this series. The magneto-optical spectra of Fe_3O_4 derive primarily from intervalence charge transfer (IVCT) and intersublattice charge transfer (ISCT) electronic transitions.[26,36] For the range 400-500 nm, observed Faraday rotation is large indicating the characteristic feature associated with all ferrites, an IVCT between M^{2+} and Fe^{3+}.[26,36] This phenomenon occurs as the result of an octahedral M^{2+} absorbing a photon and promoting the short-term transfer of an electron to a neighboring tetrahedral Fe^{3+} quickly loses the electron back to M^{2+} and the process repeats as more photons are absorbed. When $x < 4$, this region is dominated by an $Fe^{2+} \leftrightarrow Fe^{3+}$ transfer that returns a negative Faraday rotation, whereas the corresponding cobalt transition returns the opposite orientation above x=4 and has a maximum around 340 nm.[37] There is also an ISCT between Fe^{3+} ions around 475 nm.[37] Moving towards the IR (longer wavelengths), a prominent maximum centered around 550 nm emerges, for $0.2 \leq x \leq 0.4$, which diminishes as $x \rightarrow 1$. Possible causes of this feature will be discussed following the identification of all known transitions. For $x \geq 0.4$, slight shoulder appears next

around 625 nm which is attributed to an IVCT between Co^{2+} and Fe^{3+} with both on octahedral sites.[24,26] For wavelengths longer than ~700 nm, the spectra for x = 0, 0.2, and 1.0 indicate almost zero rotation of the plane of polarization while the $0.4 \leq x \leq 0.8$ samples in the series exhibit a very noticeable feature around 750 nm which is due to a CF transition from the double degenerate ground state of tetrahedrally coordinated Co^{2+}. The emergence and disappearance of this feature as x approaches 1 suggests that nearly all Co^{2+} is octahedral in pure $CoFe_2O_4$. As we have shown that Co^{2+} resides in both tetrahedral and octahedral coordination this series, the options for the unknown peak around 550 nm must now be discussed. The possible reasons for this feature may seem to be many, but in fact may be reduced to but three in the visible region: an ISCT between two Co^{2+} ions or a CF transition from a tetrahedral Fe^{3+} or octahedral Co^{2+}. Any IVCT between the two divalent species should occur at energies beyond our range. While Fe^{3+} is forbidden to undergo CF transitions,[36] this mechanism would seem to be entirely possible for Co^{2+} as increasing x decreases the symmetry of the cobalt octahedron, and thus allows CF transitions from an octahedral site.[36] It must be noted that the region around 550 nm (Fig. 4.4) is a very prominent peak which is most likely not associated with an octahedral CF transition because these are still symmetry forbidden. With all other sources discarded, we conclude that the broad peak around 550 nm must be associated with an ISCT between two Co^{2+} ions on different lattice sites. This result is consistent with the rest of our observations and leads to the conclusion that we have, indeed, formed the correct product by ratio, but the coordination of cobalt is extremely sensitive to concentration.[37,38] It seems that $Co_xFe_{1-x}Fe_2O_4$ undergoes a structural change as x increases, where Co^{2+} almost exclusively prefers the octahedral site (inverse spinel) at higher concentrations and a mix of both sites for lower concentrations.

CHAPTER 6 - CONCLUSION

A cheap, simple procedure has been developed here capable of producing fine nanopowders with tunable magnetizations from 30-50 emu/g at 10000 G by adjusting the Co^{2+}/Fe^{2+} ratio in ferrite compounds. Manipulating this ratio also allows control of the degree and orientation of Faraday by a sample. Applying the information gathered from the techniques employed, the target product has been formed, but with its structure dependent on this ratio. We have observed a tendency for cobalt to migrate to the octahedral positions at higher ratios and occupy both sites at lower ones which has resulted in the identification of an ISCT between cobalt ions around 550 nm. This migration to the octahedral site is effectively a high-spin, low-spin crossover by divalent cobalt cations as a function of concentration. Magnetic and magnetic-optical measurements have been used in this study to gather essential information concerning the spatial orientations of cations in this compound; a structural parameter that is difficult to obtain by other methods.

REFERENCES

[1] W. Reim and J. Schoenes, in *Ferromagnetic Materials, Vol. 5*, edited by K. Buschow and E. Wohlfarth (Elsevier Science, Amsterdam, 1990), Vol. 5, pp. 134-236.

[2] A.K. Zvezdin and V.A. Kotov, *Modern Magnetooptics and Magnetooptical Materials*. (Institute of Physics Publishing, London, 1997).

[3] V.A.M. Brabers, in *Handbook of Magnetic Materials*, edited by K.H.J. Buschow (Elsevier Science, Amsterdam, 1995), Vol. 8, pp. 189.

[4] D. Jiles, *Introduction to Magnetism and Magnetic Materials*. (Chapman & Hall/CRC, Boca Raton, 1998).

[5] K. Shinagawa, in *Magneto-Optics*, edited by S. Sugano and N. Nojima (Springer, Berlin, 2000).

[6] Y.P. He, Y.M. Miao, C.R. Li, S.Q. Wang, L. Cao, S.S. Xie, G.Z. Yang, B.S. Zou, and C. Burda, "Size and structure effect on optical transitions of iron oxide nanocrystals," Phys. Rev. B. **71**, 125411 (2005).

[7] A.K. Giri, E.M. Kirkpatrick, P. Moongklamklang, S.A. Majetich, and V. Harris, "Photomagnetism and structure in cobalt ferrite nanoparticles," Appl. Phys. Lett. **80**, 2341-2343 (2002).

[8] D.A. Smith, Yu. A. Barnakov, B.L. Scott, S.A. White, and K. L. Stokes, "Magneto-optical spectra of closely-spaced magnetite nanoparticles," JAP **97**, 10M504 (2005).

[9] D.A. Smith and K. L. Stokes, "Discrete dipole approximation for magneto-optical scattering calculations," Opt. Express **14**, 5746-5754 (2006).

[10] A. V. Ramos, J.-B. Moussy, M.-J. Guittet, M. Gautier-Soyer, C. Gatel, P. Bayle-Guillemaud, B. Warot-Fonrose, and E. Snoeck, "Influence of a metallic or oxide top layer in epitaxial magnetic bilayers containing $CoFe_2O_4$(111) tunnel barriers," Phys. Rev. B. **75**, 224421 (2007).

[11] A. V. Ramos, M.-J. Guittet, J.-B. Moussy, R. Mattana, C. Deranlot, F. Petroff, and C. Gatel, "Room temperature spin filtering in epitaxial cobalt-ferrite tunnel barriers," Appl. Phys. Lett. **91**, 122107 (2007).

[12] K.H.J. Buschow and F.R. DeBoer, *Physics of Magnetism and Magnetic Materials*. (Kluwer Academic/Plenum, New York, 2003).

[13] J.E. Huheey, E.A. Keiter, and R.L. Keiter, *Inorganic Chemistry: Principles of Structure and Reactivity, 4/E*. (Prentice Hall, New York, 1993).

[14] J. C. Slonczewski, "Origin of magnetic anisotropy in cobalt-substituted magnetite," Phys. Rev. **110**, 1341 - 1348 (1958).

[15] S. Li, V.T. John, C.J. O'Connor, V. Harris, and E. Carpenter, "Cobalt-ferrite nanoparticles: Structure, cation distributions, and magnetic properties," J. Appl. Phys. **87**, 6223-6225 (2000).

[16] T. Meron, Y. Rosenberg, Y. Lereah, and G. Markovich, "Synthesis and assembly of high-quality cobalt ferrite nanocrystals prepared by a modified sol–gel technique," J. Magn. Magn. Mater. **292**, 11-16 (2005).

[17] J.-S. Jung, K.-H. Choi, S.-L. Oh, Y.-R. Kim, S.-H. Lee, D. A. Smith, K.L. Stokes, L. Malkinski, and C.J. O'Connor, "$CoFe_2O_4$ nanostructures with high coercivity," J. Appl. Phys. **97**, 10F306 (2005).

[18] D. Caruntu, Y. Remond, N. H. Chou, M.-J. Jun, G. Caruntu, J. He, G. Goloverda, C. O'Connor, and V. Kolesnichenko, "Reactivity of 3d Transition Metal Cations in Diethylene Glycol Solutions. Synthesis of Transition Metal Ferrites with the Structure of Discrete Nanoparticles Complexed with Long-Chain Carboxylate Anions," Inorg. Chem. **41**, 6137-6146 (2002).

[19] D. Caruntu, G. Caruntu, Y. Chen, C.J. O'Connor, G. Goloverda, and V.L. Kolesnichenko, "Synthesis of Variable-Sized Nanocrystals of Fe_3O_4 with High Surface Reactivity," Chem. Mater., 5527-5534 (2004).

[20] E. Hecht, *Optics, 4th edition*. (Addison Wesley, San Fransisco, 2002).

[21] J.D. Jackson, *Classical Electrodynamics*, 3rd ed. (John Wiley and Sons, Inc., New York, 1999).

[22] P.S. Pershan, "Magneto-optical effects," J. Appl. Phys. **38**, 1482-1490 (1967).

[23] Z.Q. Qui and S. D. Bader, "Surface magneto-optical Kerr effect," Rev. Sci. Instrum. **71**, 1243-1255 (2000).

[24] W.F.J. Fontijin, P.J. van der Zaag, M.A.C. Devillers, V.A.M. Brabers, and R. Metselaar, "Optical and magneto-optical polar Kerr rotation spectra of Fe_3O_4 and Mg^{2+}- or Al^{2+}-substituted Fe_3O_4," Phys. Rev. B. **56**, 5432-5442 (1997).

[25] W.F.J. Fontijn, P.J. van der Zaag, and R. Metselaar, "On the origin of the magneto-optical effects in Li, Mg, Ni, and Co ferrite," J. Appl. Phys. **83**, 6765-6767 (1998).

[26] W.F.J. Fontijn, P.J. van der Zaag, and L.F. Feiner, "A consistant interpretation of the magneto-optical spectra of spinel-type ferrites," J. Appl. Phys. **85**, 5100-5105 (1999).

[27] B.P. MacPherson, P. V. Bernhardt, A. Hauser, S.Pagès, and E. Vauthey, "Time-Resolved Spectroscopy of the Metal-to-Metal Charge Transfer Excited State in Dinuclear Cyano-Bridged Mixed-Valence Complexes," Inorg. Chem. **44**, 5530-5536 (2005).

[28] K. Nassau, *The Physics and Chemistry of Color, 2nd edition*. (Wiley-Interscience, New York, 2001).

[29] Yu. A. Barnakov, B.L. Scott, V. Golub, L.A. Kelly, V. Reddy, and K.L. Stokes, "Spectral dependence of Faraday rotation in magnetite-polymer nanocomposites," J. Phys. Chem. Solids **65**, 1005-1010 (2004).

[30] P.J. Goodhew, J. Humphreys, and R. Beanland, *Electron Microscopy and Analysis, 3rd Edition*. (Taylor and Francis, New York, 2001).

[31] S.M. Dennis, M.S. Thesis, University of New Orleans, 2001.

[32] S. Mitra, K. Mandal, and P.A. Kumar, "Temperature dependence of magnetic properties of $NiFe_2O_4$ nanoparticles embeded in SiO_2 matrix," J. Magn. Magn. Mater. **306**, 254-259 (2006).

[33] H. M. Lu, W.T. Zheng, and Q. Jiang, "Saturation magnetization of ferromagnetic and ferrimagnetic nanocrystals at room temperature," J. Phys. D: Appl. Phys. **40**, 320-325 (2007).

[34] D. R. Lide, *Handbook of Chemistry and Physics, 83rd Edition*, (CRC Press, Boca Raton, 2002), pp. 12-14.

[35] L. Stichauer, G. Gavoille, and Z. Simsa, "Optical and magneto-optical properties of nanocrystalline cobalt ferrite films," J. Appl. Phys. **79**, 3645-3650 (1996).

[36] W.D. Martens, W. L. Peeters, and H.M. van Noort M. Erman, "Optical, magneto-optical and Mossbauer spectroscopy on Co^{3+} substituted cobalt ferrite," J. Phys. Chem. Solids **46**, 411-416 (1985).

[37] K.J. Kim, H.S. Lee, M.H. Lee, and S.H. Lee, "Comparative magneto-optical investigation of *d–d* charge–transfer transitions in Fe_3O_4, $CoFe_2O_4$, and $NiFe_2O_4$," J. Appl. Phys. **91**, 9974-9977 (2002).

[38] S.-H. Wei and S.B. Zhang, "First-principles study of cation distribution in eighteen closed-shell $A^{II}B_2^{III}O_4$ and $A^{IV}B_2^{II}O_4$ spinel oxides," Phys. Rev. B. **63**, 045112 (2001).

VITA

Byron L. Scott was born May 28, 1980 in Cullman, AL and relocated to Pascagoula, MS later that year. He enrolled in the University of New Orleans in fall 2000 where he received his B. S. in Chemistry in May 2003. He will receive his M. S. in Applied Physics from the University of New Orleans in December 2007.